

UC Irvine

UC Irvine Previously Published Works

Title

Energy-Efficient Resource Allocation for Fractional Frequency Reuse in Heterogeneous Networks

Permalink

<https://escholarship.org/uc/item/080674sm>

Journal

IEEE Transactions on Wireless Communications, 14(10)

ISSN

1536-1276

Authors

Davaslioglu, Kemal
Coskun, Cemil Can
Ayanoglu, Ender

Publication Date

2015

DOI

10.1109/twc.2015.2438826

Copyright Information

This work is made available under the terms of a Creative Commons Attribution License, available at <https://creativecommons.org/licenses/by/4.0/>

Peer reviewed

Energy-Efficient Resource Allocation for Fractional Frequency Reuse in Heterogeneous Networks

Kemal Davaslioglu, *Student Member, IEEE*, Cemil Can Coskun, *Student
Member, IEEE*, and Ender Ayanoglu, *Fellow, IEEE*

Center for Pervasive Communications and Computing

Department of Electrical Engineering and Computer Science

University of California, Irvine

Irvine, CA 92697-2625

Abstract

Next generation wireless networks face the challenge of increasing energy consumption while satisfying the unprecedented increase in the data rate demand. To address this problem, we propose a utility-based energy-efficient resource allocation algorithm for the downlink transmissions in heterogeneous networks (HetNets). We consider the fractional frequency reuse (FFR) method in order to mitigate the intra- and inter-cell interference. The proposed algorithm divides the resource allocation problem into frequency and power assignment problems and sequentially solves them. The proposed power control algorithm uses the gradient ascent method to control the transmit power of macrocell base stations as most of the power in the network is consumed there. We also present the optimality conditions of the resource allocation problem and the convergence of the proposed algorithm. We study the performance of the proposed algorithm in a Long Term Evolution (LTE) system. Our simulation results demonstrate that the proposed algorithm provides substantial improvements in the energy efficiency and throughput of the network.

This work was partially supported by the National Science Foundation under Grant No. 1307551. Any opinions, findings, and conclusions or recommendations expressed in this material are those of the authors and do not necessarily reflect the view of the National Science Foundation.

Index Terms

Energy efficiency, heterogeneous cellular networks, power control, Long Term Evolution (LTE), OFDM.

I. INTRODUCTION

Energy efficiency is an important issue in the next generation wireless networks. In particular, the high data rate demands of the LTE and LTE-Advanced standards bring the hidden cost of increasing energy consumption. These have been studied in the literature under the topic of “Green Communications” [1]. Network operators are also seeking green solutions in order to reduce their operational expenses. Several methods have been investigated and standardized to increase the energy efficiency of the networks, see, e.g., [1]–[5]. Among these solutions, we study the FFR method in this paper to reduce both the intra- and inter-cell interference. In the FFR method, cells are divided into cell-center and cell-edge regions and orthogonal subbands are allocated in these regions. In an interference dominated region, increasing the transmit power slightly improves the throughput, but it significantly degrades the energy efficiency. The frequency allocation of the FFR method significantly increases the energy efficiency and reduces the outages.

The resource allocation problem for multicell networks has been widely investigated in the literature, see, e.g., [6]–[12]. The study in [6] finds that the network sum throughput is maximized when the radius of the cell-center region is chosen as 0.6 times the cell radius for single-layer networks employing omnidirectional antennas. A similar study is presented in [7] for two-layer networks with three and six sector antennas in which 0.61 and 0.54 times the cell radius, respectively, are determined to be the cell-center region radii that maximize the network throughput. In contrast to the studies that maximize the network throughput, in this paper, we investigate the cell-center radius that maximizes the energy efficiency, which has not been investigated in the literature. Several studies have been reported investigating energy-efficient resource allocation in multicell networks, see, e.g. [8]–[10]. These works consider the static power consumption along with the transmit power to develop better link adaptation schemes. In our paper, this problem is also addressed but in a large scale such that the energy efficiency of

the complete network is maximized. In [11], the effects of the cell-center region radius have been investigated. The authors identify that as the number of users increases the optimal cell-center radius needs to decrease. Reference [12] investigates resource allocation in time, frequency, and both time and frequency domains. Considering the complexity of the problem and practical constraints, [12] proposes to use constant energy across subbands instead of using a multi-user water-filling algorithm. It needs to be noted that the same constraints also apply to the LTE and LTE-Advanced systems, where the standards define the smallest scheduling granularity to be per resource block and constant power is allocated to the subcarriers within a resource block [2]. In this paper, we also employ this approach and find the optimal power levels that maximize the energy efficiency of the network. A recent study in [7] proposed a novel FFR scheme for HetNet deployments with sectorized macrocell base stations, we use the same scheme.

In this paper, we address the resource allocation problem in Orthogonal Frequency Division Multiple Access (OFDMA) systems employing the FFR method in HetNets deployments. We propose a novel resource allocation algorithm in which the objective is to maximize the energy efficiency in each sector. We account for both the transmit and static power consumed at base stations. The proposed algorithm divides the resource allocation problem into frequency and power allocation problems. To solve the frequency assignment problem, we investigate two well-known schedulers, the sum rate maximization (SRM) and equal bandwidth (EBW) schedulers [13]. For the power control assignments, the gradient ascent method is applied. We note that power control is applied only at the macrocell base station (MeNB) and not at the picocell base station (pico eNB) in order to eliminate excessive traffic overhead among base stations, which is especially critical as the network becomes denser with small cell deployments. This also makes sure that full coverage is provided in the small cells.

The remainder of this paper is organized as follows. Section II introduces the system model and presents the base station power consumption models. Section III formulates the energy-efficient resource allocation problem in OFDMA systems employing the FFR method. The proposed algorithm is presented in Section III, along with the optimality conditions and the convergence proof of the proposed algorithm. Numerical results demonstrating the performance improvements

are presented in Section IV and concluding remarks are made in Section V.

II. SYSTEM MODEL

In this section, we first present the FFR method used in this paper. Then we identify the interference conditions in each region and present the system model. Finally we discuss the base station power consumption models that are used to derive energy-efficient algorithms.

Interference is a key problem in mobile wireless communication systems. In today's mobile communication networks, base station distances are typically on the order of less than a kilometer for urban deployments. This poses a challenging interference problem for HetNet deployments due to the large downlink transmit power differences. For example, the MeNBs and pico eNBs differ by 16 dB in their transmit power levels [2], [14]. In order to mitigate interference, several methods have been proposed such as FFR [7], enhanced inter-cell interference cancellation [2], coordinated multipoint transmissions [15], and carrier aggregation [2]. In the FFR method, different subbands are allocated in different geographical regions. Each cell is divided into two regions as the cell-center and cell-edge region. Depending on the locations, the macrocell and picocell associated users, abbreviated as MUEs and PUEs, respectively, are assigned to different subbands. This orthogonal frequency assignment significantly reduces both the intra- and inter-cell interference. In this paper, we denote the cell-center region radius as r_{th} . This distance sets the region boundaries. For example, users that are closer than r_{th} to the MeNB are considered to be in the cell-center region and those that are farther are considered to be in the cell-edge region. Similarly, users connected to a pico eNB located closer than r_{th} to the MeNB are considered to be in the cell-center region.

Consider the FFR scheme depicted in Fig. 1. In the macrocell tier, the system bandwidth is partitioned into subbands such that subband A is assigned to the cell-center region for the macrocell tier, and the rest of the spectrum is divided into three subbands, one for each sector. In the picocell tier, two of these subbands are allocated to the PUEs in the cell-center region, while subband A is also available for those in the cell-edge region. Due to different spectrum allocations, interference conditions vary depending on the cell region and the associated tier. Let us identify the interference conditions for the MUEs and PUEs in the cell-center and cell-edge

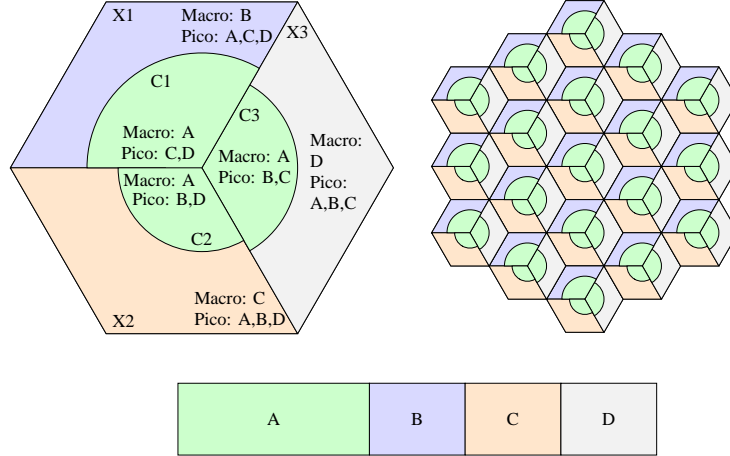


Figure 1. A multi-tier FFR scheme with dynamic cell-center region boundaries is depicted in a uniform hexagonal grid of 19 cells. The MeNBs employ three sector antennas, whereas pico eNBs have omnidirectional antennas.

regions of each sector. For example, in Sector 1, the MUEs in the cell-center region are assigned to subband A , while the PUEs in the same region are allocated to subbands C and D . On the other hand, in the cell-edge region, the MUEs are scheduled on subband B , whereas the PUEs operate on subbands A , C , and D .

First, consider the MUEs in the cell-center region that are scheduled on subband A . The strongest interfering base stations for the users in this region are the six MeNBs in the first ring surrounding this cell. Also, note that the surrounding 12 MeNBs in the second ring create interference although at smaller magnitudes. As for the cross-tier interference, the picocells transmitting on subband A located in the cell-edge region create interference for these users. Then, we can express the signal-to-interference-plus-noise ratio (SINR) of an MUE k in the cell-center region on subcarrier n as

$$\gamma_k^{(n)} = \frac{P_M^{(n)} g_{k,b}^{(n)}}{\sum_{b' \in \mathcal{B}_M^A, b' \neq b} P_M^{(n)} g_{k,b'}^{(n)} + \sum_{b'' \in \mathcal{B}_P^A} P_P^{(n)} g_{k,b''}^{(n)} + N_0 \Delta_f} \quad (1)$$

where $P_M^{(n)}$ and $P_P^{(n)}$ denote the downlink transmit powers of macrocell M and picocell P on subcarrier n , respectively. The channel gain between user k and base station b is denoted by $g_{k,b}^{(n)}$ on subcarrier n . Also, \mathcal{B}_M^A and \mathcal{B}_P^A denote the set of MeNBs and pico eNBs operating on

subband A . The thermal noise power per Hz is denoted by N_0 . The bandwidth of a subcarrier is represented as Δ_f , $\Delta_f = 15$ kHz for LTE systems [2].

Similarly, we can express the SINR of the MUEs in the cell-edge region of Sector 1 as

$$\gamma_k^{(n)} = \frac{P_M^{(n)} g_{k,b}^{(n)}}{\sum_{b' \in \mathcal{B}_M^B, b' \neq b} P_M^{(n)} g_{k,b'}^{(n)} + \sum_{b'' \in \mathcal{B}_P^B} P_P^{(n)} g_{k,b''}^{(n)} + N_0 \Delta_f} \quad (2)$$

where \mathcal{B}_M^B and \mathcal{B}_P^B are the set of MeNBs and pico eNBs operating on subband B , respectively. Note that in this region, the number of interfering MeNBs in the first ring is reduced from six to two due to the frequency reuse of 1/3. This comes from the sectorization at the MeNBs. As in the cell-center region, the picocells operating on subband B still interfere with the MUEs in the cell-edge region. The five MeNBs in the second ring also create interference, but relatively less compared to those from the first tier. It is straightforward to derive the interference conditions for the cell-center and cell-edge MUEs in Sectors 2 and 3, and these are omitted due to space considerations.

Let us now discuss the interference conditions for the PUEs. Assume that a PUE k is located in the cell-center region of Sector 1. This user can be scheduled on the resources over the subbands C and D . The interference from the picocell tier comes from the pico eNBs operating over these subbands. These correspond to the pico eNBs within the same cell and those in the neighboring cells. The interference from the macrocell tier is mainly caused by the four MeNBs in the first ring, in which each MeNB creates interference for either one of these subbands. Note that the closest MeNB does not interfere with the pico eNBs in the cell-center region as they are allocated to different subbands. Hence, this spectrum allocation significantly decreases the number of interfering MeNBs for the picocell tier, and thereby reduces the cross-tier interference. Following our previous notation, the SINR of a PUE in the cell-center region scheduled to the subcarriers in subband C is given by

$$\gamma_k^{(n)} = \frac{P_P^{(n)} g_{k,b}^{(n)}}{\sum_{b' \in \mathcal{B}_M^C} P_M^{(n)} g_{k,b'}^{(n)} + \sum_{b'' \in \mathcal{B}_P^C, b'' \neq b} P_P^{(n)} g_{k,b''}^{(n)} + N_0 \Delta_f} \quad (3)$$

where \mathcal{B}_M^C and \mathcal{B}_P^C denote the set of MeNBs and pico eNBs operating on subband C . Similar

expressions can be obtained for the other PUEs, in which the only differences will be the interfering base stations.

Constant power allocation over subbands is considered in this paper, which follows the standards for LTE systems [2]. The proposed algorithm in Section III-A introduces two power control parameters β and ε to adjust the downlink transmit power levels. The first parameter β scales the transmit power of each MeNB. The second parameter ε denotes the ratio of the power allocated to the subcarriers in the cell-edge region to those in the cell-center region. By this way, ε characterizes the fairness between the MUEs in the cell-center and cell-edge regions. Let N_A , N_B , N_C , and N_D denote the total number of subcarriers in subbands A , B , C , and D , respectively. Then, for Sector 1, the maximum transmit power of an MeNB satisfies

$$\beta P_{\max,M} = P_M N_A + \varepsilon P_M N_B, \quad (4)$$

and therefore

$$P_M = \frac{\beta P_{\max,M}}{N_A + \varepsilon N_B} \quad (5)$$

where P_M and $P_{\max,M}$ are the MeNB transmit power per subcarrier in the cell-center region and the MeNB maximum transmit power, respectively. The term εP_M denotes the transmit power per subcarrier for the MUEs in the cell-edge region. Similar expressions can be obtained for Sectors 2 and 3 by replacing N_B with N_C and N_D , respectively. For completeness, we also express the picocell transmit power per subcarrier. For a pico eNB in Sector 1, the transmit power per subcarrier, denoted by P_P , depends on the picocell's location in the cell, and it is given by

$$P_P = \begin{cases} P_{\max,P} / (N_C + N_D) & \text{if } d_p \leq r_{th} \\ P_{\max,P} / (N_A + N_C + N_D) & \text{if } d_p > r_{th} \end{cases} \quad (6)$$

where P_P and $P_{\max,P}$ are the transmit power of a pico eNB per subcarrier and the maximum transmit power of a pico eNB, respectively. The distance between the closest macrocell and the pico eNB is denoted by d_p . Similar expressions can be obtained for Sectors 2 and 3 by replacing

N_C with N_B and N_D with N_B , respectively.

A. Base Station Power Consumption Models

Recent studies have quantified the energy consumption of a base station down to the component level and several power consumption models have been proposed, see, e.g., [16]–[18]. These models include the contributions of the power amplifier, radio frequency (RF) transceiver parts, baseband unit, power supply, and cooling devices [16]. Using these models each component's contribution can be identified and efficient methods can be developed to introduce energy savings [1]. In this paper, we study the load-dependent power consumption model presented in [16], which is given by

$$P_{Total} = \begin{cases} N_{TRX} (P_0 + \Delta \cdot P_{TX}) & 0 < P_{TX} \leq P_{max} \\ N_{TRX} P_{sleep} & P_{out} = 0 \end{cases} \quad (7)$$

where P_{Total} and P_{TX} are the overall base station power consumption and RF transmit output powers, respectively. N_{TRX} is the number of transceiver chains, P_0 is the power consumption at the minimum non-zero output power, and Δ is the slope of the load-dependent power consumption. P_{sleep} denotes the power consumption of the sleep mode. Notice that the power consumption at a base station depends on the RF transmit power, P_{TX} , and thereby this model is referred to as load-dependent power consumption model. Using this definition, the power consumption at an MeNB and a pico eNB can be expressed as

$$P_{Macro} = N_{TRX,M} (P_{0,M} + \Delta_M P_{TX,M}) \quad \text{and} \quad P_{Pico} = N_{TRX,P} (P_{0,P} + \Delta_P P_{TX,P}) \quad (8)$$

where $P_{0,M}$, $P_{0,P}$, P_{Macro} , and P_{Pico} are the power consumption at the minimum non-zero output power and the total power consumption of the MeNBs and pico eNBs, respectively. $N_{TRX,M}$ and $N_{TRX,P}$ represent the number of transceiver chains at the MeNBs and pico eNBs, respectively. The corresponding slopes of the load-dependent power consumption are denoted as Δ_M and Δ_P , in the same order as before. Note that (8) is true for $0 < P_{TX,M} \leq P_{max,M}$ and $0 < P_{TX,P} \leq P_{max,P}$, where $P_{max,M}$ and $P_{max,P}$ are the maximum RF transmit power for MeNBs and pico eNBs, respectively. If $P_{TX,M} = 0$ (or $P_{TX,P} = 0$), then $P_{Macro} = N_{TRX,M} P_{sleep,M}$ (or

Table I
BASE STATION POWER CONSUMPTION MODEL PARAMETER VALUES [16]

Base Station Type	P_0 (W)	P_{sleep} (W)	P_{max} (W)	Δ
MeNB	130	75.0	20	4.7
Pico eNB	56	39.0	6.3	2.6

$P_{Pico} = N_{TRX,P}P_{sleep,P}$), where $P_{sleep,M}$ and $P_{sleep,P}$ are the power consumption of the sleep modes of MeNBs and pico eNBs, respectively. Table I presents the corresponding parameter values of the linearized power consumption model for various base station types.

III. ENERGY-EFFICIENT RESOURCE ALLOCATION PROBLEM

In this section, we formulate a non-cooperative resource allocation problem in OFDM systems employing the FFR method. Our objective is to maximize the energy efficiency per sector by determining the optimal resource block allocation and the optimal power level assignment on each subband. In the sequel, we define the energy efficiency per sector, formulate the problem, and present its complexity analysis. Then, we proceed to propose our algorithm, along with its complexity analysis, optimality conditions, and convergence analysis.

Let $R_k(\gamma_k)$ denote the throughput of user k that depends on its SINR γ_k . Also, let $\mathcal{K}_{M,i}^C$, $\mathcal{K}_{M,i}^X$, $\mathcal{K}_{P,i}^C$, and $\mathcal{K}_{P,i}^X$ denote the set of MUEs in sector i connected to the MeNB in the cell-center and cell-edge regions, and the set of PUEs connected to the pico eNBs in the cell-center and cell-edge regions of this sector, respectively. Note that the subscript i denotes the sector indices. Then, the energy efficiency per sector i is given by

$$\eta_{EE,i} = \frac{\sum_{k \in \mathcal{K}_{M,i}^C \cup \mathcal{K}_{M,i}^X} R_k(\gamma_k) + \sum_{k \in \mathcal{K}_{P,i}^C \cup \mathcal{K}_{P,i}^X} R_k(\gamma_k)}{\psi_i} \quad (9)$$

where the total power consumed per sector i is denoted by ψ_i which can be expressed as

$$\psi_i = N_{TRX,M,i} (P_{0,M} + \Delta_M P_{TX,M}) + N_{picos} N_{TRX,P,i} (P_{0,P} + \Delta_P P_{TX,P}) \quad (10)$$

where N_{picos} is the number of picocells in sector. The energy efficiency is given in units of

bits/Joule.

The energy-efficient resource allocation problem can be formulated as

$$\max_{\mathbf{F}, \mathbf{P}_M, \mathbf{P}_P} \eta_{EE,i} \quad (11)$$

where \mathbf{F} denotes the resource block allocation vector, and \mathbf{P}_M and \mathbf{P}_P are the MeNB and pico eNB power assignment vectors. The solution requires a joint search over the frequency and power domains. It is shown in [12] that the optimal solution is the multilevel water-filling solution. However, finding the optimal resource block assignments among K users and N_{RB} resource blocks requires $K^{N_{RB}}$ searches [12]. Therefore, this approach is impractical for real applications and it can lead to large latencies in practice as there are more users in the system. In the next subsection, we present our proposed algorithm that divides the resource allocation problem into two stages decoupling the frequency and power allocation problems.

A. Proposed Solution

Obtaining the instantaneous interference conditions of the complete network is often impractical for real applications due to excessive traffic overhead it would require. Therefore, recent studies have focused on non-cooperative or clustered base station resource allocation algorithms in multicell systems, see, e.g., [9], [10], and Chapter 11 of [2]. In this paper, we investigate a non-cooperative solution in which each MeNB sector maximizes its own energy efficiency. We assume that there is a fast and reliable information exchange between the MeNB and the pico eNBs in the same sector such that the channel conditions of the PUEs are known at the MeNB. In LTE and LTE-Advanced, this is exchanged over the X2 interface [2].

The proposed algorithm starts with determining the cell-center region boundaries. We propose two different algorithms which are described below. Then, we decouple the frequency and power allocation problems into two stages. First, we solve the frequency assignment problem. Once these are obtained, we assign the power levels that maximize the energy efficiency at each sector.

1) *Setting The Cell-Center Region Boundaries:* The cell-center region radius per sector, r_{th} , is an important design parameter that affects the system performance in OFDMA systems employing the FFR method. It determines the set of MUEs and PUEs in the cell-center and

cell-edge regions. Once these regions are defined, the picocells that are located in each region can be identified as well. Considering the spatial and temporal variations of the user distribution in each cell, this parameter needs to be dynamically adjusted per sector. For this purpose, we study two algorithms. The first algorithm maximizes the sector throughput, whereas the second one increases the fairness.

In the first algorithm, the MUE with the lowest path loss, that is the closest MUE to the MeNB, is selected to be in the cell-center region, while the rest of the MUEs are assigned to the cell-edge region subbands. The SINR of this user is expected to be greater than the other MUEs because it has the lowest path loss and it is farthest away from the neighboring MeNBs. Consequently, the cell-center region subbands are allocated to only one MUE maximizing its throughput. In general, this algorithm achieves the maximum throughput at the cost of system fairness. We refer to this algorithm as Adaptive R_{th} Algorithm 1.

In the second algorithm, the cell-center region boundary is determined such that the ratio of cell-center and cell-edge MUEs is proportional to the ratio of the subbands allocated in these regions. First, the MUEs are sorted in ascending order based on their path losses. Let N_M^C and N_M^X denote the number of subcarriers that the MeNB uses in the cell-center and cell-edge regions. For K MUEs in sector i , we round $(N_M^C / (N_M^C + N_M^X) \cdot K)$ to the nearest integer, and $\lfloor 0.5 + N_M^C / (N_M^C + N_M^X) \cdot K \rfloor$ users are considered in the cell-center region. The rest of the users are assigned to the cell-edge subbands. This achieves higher fairness, but this comes at the cost of a decrease in the sector throughput. We refer to this algorithm as Adaptive R_{th} Algorithm 2. Note that a similar method is proposed in [19] to determine the cell-center boundaries.

2) *Frequency Assignment Problem:* In order to solve the frequency assignment problem we study two schedulers. First, we study the SRM scheduler discussed in [13]. In this scheduler, the resource blocks are assigned to users such that the throughput is maximized. This scheduler is investigated to maximize the throughput, although this comes at the cost of a decrease in the system fairness. The second scheduler we study is the EBW scheduler. Consider K users sharing N_{RB} resource blocks. Then, $K_h = \text{mod}(N_{RB}, K)$ users get $\lfloor N_{RB}/K \rfloor + 1$ resource blocks, whereas $K_i = K - K_h$ users are given $\lfloor N_{RB}/K \rfloor$ resource blocks. This scheduler is discussed

in [14] to calibrate system level simulations.

3) *Power Assignment Problem*: Second stage of the proposed algorithm solves the power assignment problem by assigning the optimal power levels to the subbands. The proposed algorithm uses the gradient ascent method to solve this problem. First we observe that by controlling the transmissions for the MUEs in the cell-center region, we also determine how much interference is created for the PUEs in the cell-edge region. Similarly, the downlink transmissions for the MUEs in the cell-edge region determines the interference for the PUEs in the cell-center region. In order to capture these two effects, we introduce two variables into the optimization problem as β and ε , as discussed earlier in Section II.

Consider the following function $\eta_i(\varepsilon, \beta)$ that only includes the throughput of users in sector i that are affected by the optimization variables ε and β . Those users are the MUEs in both regions and the PUEs in the cell-edge region. While calculating $\eta_i(\varepsilon, \beta)$ only the interference created within each sector is considered. The energy efficiency function in sector i can be modified as

$$\eta_i(\varepsilon, \beta) = \frac{\sum_{k \in \mathcal{K}_{M,i}^C} R_k(\gamma_k) + \sum_{k \in \mathcal{K}_{M,i}^X} R_k(\gamma_k) + \sum_{k \in \mathcal{K}_{P,i}^X} R_k(\gamma_k)}{\psi_i} \quad (12)$$

where $R_k(\gamma_k)$ denotes the user capacity of the corresponding region and tier associations. The power consumed in sector i is denoted by ψ_i . We modify (10) to account for the power control parameter β such that ψ_i can be expressed as

$$\psi_i = N_{TRX,M,i} (P_{0,M} + \Delta_M \beta P_{\max,M}) + N_{\text{picos}} N_{TRX,P,i} (P_{0,P} + \Delta_P P_{\max,P}). \quad (13)$$

Hence, β can be used to introduce energy savings in the total RF transmit power.

The energy efficiency per sector definition in (12) can be expanded as

$$\begin{aligned} \eta_i(\varepsilon, \beta) = \Delta f & \frac{\sum_{k \in \mathcal{K}_{M,i}^C} \sum_{n \in \mathcal{N}_{M_k}^C} \log_2 \left(1 + \frac{\beta P_{\max,M} g_{k,m}^{(n)}}{(N_M^C + \varepsilon N_M^X) I_k^{(n)}} \right) + \sum_{k \in \mathcal{K}_{M,i}^X} \sum_{n \in \mathcal{N}_{M_k}^X} \log_2 \left(1 + \frac{\beta \varepsilon P_{\max,M} g_{k,m}^{(n)}}{(N_M^C + \varepsilon N_M^X) N_0 \Delta_f} \right)}{\psi_i} \\ & + \Delta f \frac{\sum_{k \in \mathcal{K}_{P,i}^X} \sum_{n \in \mathcal{N}_{P_k}^X \cap \mathcal{N}_M^C} \log_2 \left(1 + \frac{P_{\max,P} g_{k,p}^{(n)} / N_P^X}{\frac{\beta P_{\max,M} g_{k,M}^{(n)}}{N_M^C + \varepsilon N_M^X} + N_0 \Delta_f} \right)}{\psi_i} \end{aligned} \quad (14)$$

where $I_k^{(n)}$ is the interference from the picocells using subband A in cell-edge region plus the thermal noise effective over a subcarrier at the PUE. The expression $n \in \mathcal{N}_{P_k}^X \cap \mathcal{N}_M^C$ in (14) denotes the subcarriers that the downlink transmissions of the cell-center MUEs creates interference for the cell-edge PUEs, which are the subcarriers in subband A for the FFR scheme in Fig. 1. It needs to be emphasized that (14) considers only the intracell interference and not the inter-cell interference. This enables fast implementation as it does not necessitate information exchange between MeNBs and asynchronous implementation at each MeNB sector. For that reason, this type of formulation is robust against intercell backhaul transmission delays.

The optimization problem that maximizes the energy efficiency per sector can be written as

$$\begin{aligned} \max_{\varepsilon, \beta} \quad & \eta_i(\varepsilon, \beta) \\ \text{s.t.} \quad & \varepsilon \geq 1 \\ & 0 \leq \beta \leq 1. \end{aligned} \tag{15}$$

The first constraint is to favor the MUEs in the cell-edge region such that they are transmitted at least ε times the power allocated for the MUEs in the cell-center region. This parameter also affects the interference incurred at the PUEs in the cell-edge region. The second constraint scales the total RF transmit power of the MeNB and sets the boundary conditions. Hence, the variable β not only determines the interference, but it also introduces energy savings to the system.

B. Optimality Conditions

The Lagrangian of the problem in (15) can be written as

$$\mathcal{L}(\varepsilon, \beta, \boldsymbol{\lambda}) = \eta_i(\varepsilon, \beta) + \lambda_1(1 - \varepsilon) - \lambda_2\beta + \lambda_3(\beta - 1) \tag{16}$$

where λ_1 , λ_2 , and λ_3 are the Lagrange multipliers and $\boldsymbol{\lambda} = (\lambda_1, \lambda_2, \lambda_3)$. Note that if (ε^*, β^*) solves (15), then $\eta_i(\varepsilon^*, \beta^*) \geq \eta_i(\varepsilon, \beta)$ for all $\varepsilon \geq 1$ and $0 \leq \beta \leq 1$. Furthermore, there exists

$\lambda^* \geq 0$ such that the following optimality conditions are satisfied

$$\begin{aligned} \frac{\partial \mathcal{L}(\varepsilon^*, \beta^*, \lambda^*)}{\partial \varepsilon} &= \frac{\partial \eta_i(\varepsilon^*, \beta^*)}{\partial \varepsilon} - \lambda_1^* = 0, \\ \frac{\partial \mathcal{L}(\varepsilon^*, \beta^*, \lambda^*)}{\partial \beta} &= \frac{\partial \eta_i(\varepsilon^*, \beta^*)}{\partial \beta} - \lambda_2^* + \lambda_3^* = 0, \end{aligned} \quad (17)$$

and the complementary slackness conditions are

$$(1 - \varepsilon^*)\lambda_1^* = 0, \quad \beta^*\lambda_2^* = 0, \quad (\beta^* - 1)\lambda_3^* = 0, \quad \text{and} \quad \lambda_1^*, \lambda_2^*, \lambda_3^* \leq 0. \quad (18)$$

The equations in (17)-(18) are commonly known as the Karush-Kuhn-Tucker (KKT) conditions [20]. It needs to be emphasized that the power control parameters ε and β depend on the number of resource blocks allocated to the cell-center and cell-edge regions, the channel conditions, the maximum transmit powers, and the bandwidth of each subcarrier.

C. Gradient Ascent Method

The gradient ascent method starts at an initial (ε, β) value evaluated at time t and the parameters ε and β are updated

$$\varepsilon_{t+1} = \varepsilon_t + \mu_t \nabla_{\varepsilon} \eta_i(\varepsilon_t, \beta_t) \quad \text{and} \quad \beta_{t+1} = \beta_t + \mu_t \nabla_{\beta} \eta_i(\varepsilon_t, \beta_t) \quad (19)$$

where ε_{t+1} and β_{t+1} are the updated values at time $t+1$, respectively. $\nabla_{\varepsilon} \eta_i(\varepsilon, \beta) = \partial \eta_i(\varepsilon, \beta) / \partial \varepsilon$ and $\nabla_{\beta} \eta_i(\varepsilon, \beta) = \partial \eta_i(\varepsilon, \beta) / \partial \beta$ are the partial derivatives of η_i with respect to ε and β , respectively, evaluated at time t . These partial derivatives are multiplied by a sufficiently small and positive step size μ_t . The step size at each iteration is chosen according to the Armijo rule [21]. In this rule, the step size is chosen as $\mu_t = \mu_0^m s$, where s is a constant and m is the first non-negative integer that satisfies the following inequality

$$\eta_i(\varepsilon_{t+1}, \beta_{t+1}) - \eta_i(\varepsilon_t, \beta_t) \geq \rho \mu_t \nabla \eta_i(\varepsilon_t, \beta_t)^T \mathbf{d}_t \quad (20)$$

where ρ is a fixed constant and \mathbf{d}_t is a feasible direction. The gradient is shown by $\nabla \eta_i(\varepsilon, \beta) = [\nabla_{\varepsilon} \eta_i(\varepsilon, \beta) \quad \nabla_{\beta} \eta_i(\varepsilon, \beta)]^T$, where $[\cdot]^T$ denotes the transpose operator. Starting from $m = 0$, it is successively increased until (20) is satisfied. Note that the gradient ascent method without the

Armijo rule can fail to converge to a stationary point as illustrated in [21, p. 26], but when the step size is determined with the Armijo rule, it is guaranteed that the energy efficiency per sector increases per iteration until the algorithm converges. This enables selecting the increment that sufficiently improves the current objective value. Typical values of these constants are such that $\rho \in [10^{-5}, 10^{-1}]$ and μ_0 is usually between 1/2 and 1/10 [21]. The directional vector \mathbf{d}_t is an ascent direction if it satisfies

$$\begin{aligned} \nabla \eta_i(\varepsilon_t, \beta_t)^T \mathbf{d}_t &> 0 \quad \text{if } \nabla \eta_i(\varepsilon_t, \beta_t) \neq \mathbf{0}, \\ \nabla \eta_i(\varepsilon_t, \beta_t)^T \mathbf{d}_t &= 0 \quad \text{if } \nabla \eta_i(\varepsilon_t, \beta_t) = \mathbf{0}. \end{aligned} \tag{21}$$

In this paper, we consider the steepest descent method, that is $\mathbf{d}_t = \nabla \eta_i(\varepsilon_t, \beta_t)^T$. The expressions of the partial derivatives $\nabla_\varepsilon \eta_i(\varepsilon, \beta)$ and $\nabla_\beta \eta_i(\varepsilon, \beta)$ can be found in the Appendix.

D. Convergence Analysis

In what follows, we investigate the convergence of the proposed algorithm. To this end, we first show the quasiconcavity of the objective function η_i with respect to the optimization variables ε and β . Then, we study the optimality of the solutions obtained by the gradient ascent method.

Definition 1. A function f is called *quasiconcave* if its domain, denoted by $\text{dom } f$, is convex and for any $x, y \in \text{dom } f$,

$$f(\phi x + (1 - \phi)y) \geq \min\{f(x), f(y)\} \tag{22}$$

where $0 \leq \phi \leq 1$ [20]. Similarly, a function f is called *strictly quasiconcave* if it satisfies (22) with strict inequality for $x \neq y$ and $0 < \phi < 1$ [20].

Proposition 1. (First-Order Characterization) Let $f(\mathbf{x})$ be a continuously differentiable function on an open and convex set $\mathcal{D} \subset \mathbb{R}^n$. Then, f is quasiconcave if and only if

$$f(\mathbf{y}) \geq f(\mathbf{x}) \implies \nabla f(\mathbf{x})^T (\mathbf{y} - \mathbf{x}) \geq 0, \tag{23}$$

for all $\mathbf{x}, \mathbf{y} \in \mathcal{D}$ [20].

Proposition 2. (Second-Order Characterization) *Let $f(\mathbf{x})$ be a twice differentiable function and its dimensions be denoted by n . If $f(\mathbf{x})$ is quasiconcave, then for all $\mathbf{x} \in \text{dom } f$*

$$\mathbf{y}^T \nabla^2 f(\mathbf{x}) \mathbf{y} \leq 0 \quad (24)$$

for all $\mathbf{y} \in \mathbb{R}^n$ satisfying $\mathbf{y}^T \nabla f(\mathbf{x}) = 0$ [22].

We now present a lemma and a simple proof.

Lemma 1. *Let \mathcal{D} be a nonempty convex set and f be a strictly quasiconcave function. Then, any local maximum is a global solution of the problem $P = \sup\{f(x) | x \in \mathcal{D}\}$ [22].*

Proof: Assume that $\hat{x} \in \mathcal{D}$ is a local maximum. This means that there exists a real positive number τ such that $f(x) \leq f(\hat{x})$ holds for any $x \in \mathcal{D}$ with $\|x - \hat{x}\| \leq \tau$. Let us prove by contradiction. Assume that \hat{x} is not global maximum. Then, there exists $y \in \mathcal{D}$ such that $f(y) > f(\hat{x})$ holds. Let $0 \leq \phi \leq 1$ and define $x_\phi = \phi y + (1 - \phi)\hat{x}$. The convexity of \mathcal{D} implies that $x_\phi \in \mathcal{D}$ for all $\phi \in [0, 1]$. If ϕ is small enough, we have $\|x_\phi - \hat{x}\| \leq \tau$. Using the quasiconcavity property of f , we have

$$f(x_\phi) = f(\phi y + (1 - \phi)\hat{x}) > \min\{f(\hat{x}), f(y)\} = f(\hat{x}) \quad (25)$$

which holds for a small enough and positive ϕ . However, this contradicts the assumption that \hat{x} is a local maximum. ■

In cases where the concavity (or similarly convexity) of the problem cannot be assumed, the results of Lemma 1 are important to determine global extreme points. In fact, these are directly applicable to problems in several research fields such as those in economics. We refer the reader to Appendix C.6 of [22] for an example problem in economics, the standard consumer demand problem in a deterministic framework. It needs to be emphasized that care needs to be taken in applying Lemma 1. The local extreme point of a quasiconcave (or quasiconvex) problem should not be confused with the stationary points as for determining the global extreme point. Next, using the definitions and lemmas above, we present Lemma 2, whose proof is provided in the Appendix due to its length.

Lemma 2. *The energy efficiency per sector expression η_i in (12) is strictly quasiconcave in ε and β .*

Theorem 1. *The proposed update rules for ε and β in (19) converge to the global optimal solution of the problem (15) as $t \rightarrow \infty$ for a sufficiently small step size μ_t .*

Proof: It follows from Lemma 1 that if there exists a local solution to the maximization problem, then there is a global maximum. It is straightforward to show that the solutions obtained by the gradient ascent method with sufficiently small step sizes converge to the globally maximum solution. ■

IV. NUMERICAL RESULTS

In this section, the performance of the proposed algorithm is evaluated. We quantify the individual contributions of power control, frequency scheduling, cell-center region radius, and spectrum allocation. We compare the performance of the proposed algorithm to the orthogonal and cochannel spectrum allocation methods, and demonstrate the achievable gains. In addition, we investigate three algorithms for determining the cell-center region boundaries. We investigate the Adaptive R_{th} Algorithms 1 and 2, described in Section III-A. Also, we consider the case with the fixed FFR boundaries, in which the cell radius that maximizes the average energy efficiency is chosen through enumeration methods. Note that this analysis is presented in Figs. 5 and 6. Based on this analysis, we find that when the cell-center region radius is taken as 0.3 times the cell radius, it maximizes the average energy efficiency. In terms of spectrum allocation, MeNBs and pico eNBs transmit over all subcarriers in the cochannel allocation, whereas the spectrum is divided into 32 and 18 non-overlapping resource blocks for the MeNBs and pico eNBs, respectively, in the orthogonal channel allocation. For the FFR method, there are 32 resource blocks in the subband A and 6 resource blocks are allocated to subbands B , C , and D , i.e., $N_M^C = 32$, $N_M^X = 6$, $N_P^C = 12$, and $N_P^X = 44$ [6]. The same spectrum allocation is employed for the no power control FFR algorithm case. In the cochannel and orthogonal frequency allocation methods, base stations transmit at full power and no power control algorithm has been applied.

In order to demonstrate the FFR gain over FR methods, we study two different frequency

Table II
SIMULATION PARAMETERS

Parameter	Setting
Channel bandwidth	10 MHz
Total number of data RBs	50 RBs
Freq. selective channel model (CM)	Extended Typical Urban CM
UE to macro BS PL model	$128.1 + 37.6 \log_{10}(d)$
UE to pico BS PL model	$140.7 + 36.7 \log_{10}(d)$
Effective thermal noise power, N_0	-174 dBm/Hz
UE noise figures	9 dB
Macro and Picocell BS antenna gain	14 dBi and 5 dBi
UE antenna gain	0 dBi
Antenna horizontal pattern, $A(\theta)$	$-\min(12(\theta/\theta_{3dB})^2, A_m)$
A_m and θ_{3dB}	20 dB and 70°
Penetration loss	20 dB
Macro- and picocell shadowing	8 dB and 10 dB
Inter-site distance	500 m
Minimum macro- to user distance	50 m
Minimum pico- to user distance	10 m
Minimum pico- to macro- distance	75 m
Minimum pico- to pico- distance	40 m
Traffic model	Full buffer

reuse (FR) spectrum allocation schemes in the HetNet architecture. In both FR methods, the system bandwidth is divided into three subbands, subbands A , B , and C . In the first FR method, abbreviated as FR1 in Fig. 3 and Fig. 4, each macrocell sector uses one of the three subbands, while the rest two subbands are allocated to the picocell tier. In the second FR method, abbreviated by FR2, only one subband is assigned to the macrocell and picocell tiers. Note that the FR1 method aims to maximize throughput, whereas the FR2 method is designed to reduce interference, especially at the cell-edge region.

The simulation layout is shown in Fig. 1. It assumes a HetNet deployment with 19 hexagonal cells in which MeNBs are employed with 3-sector antennas. In each sector, there is a single antenna, i.e., $N_{TRX,M,i} = 1, \forall i$. For the pico eNBs, omnidirectional antennas are employed, i.e., $N_{TRX,P,i} = 1, \forall i$. There are 4 randomly placed pico eNBs in each sector. In order to observe the clustering effects and potential energy savings, we consider nonuniform user distribution and generate 20 users per sector. First, we place one user per pico eNB within a 40 meter radius, while the rest of the users are randomly generated within the sector area. The users are associated to the base stations with the highest reference signal received power (RSRP) method [23]. While

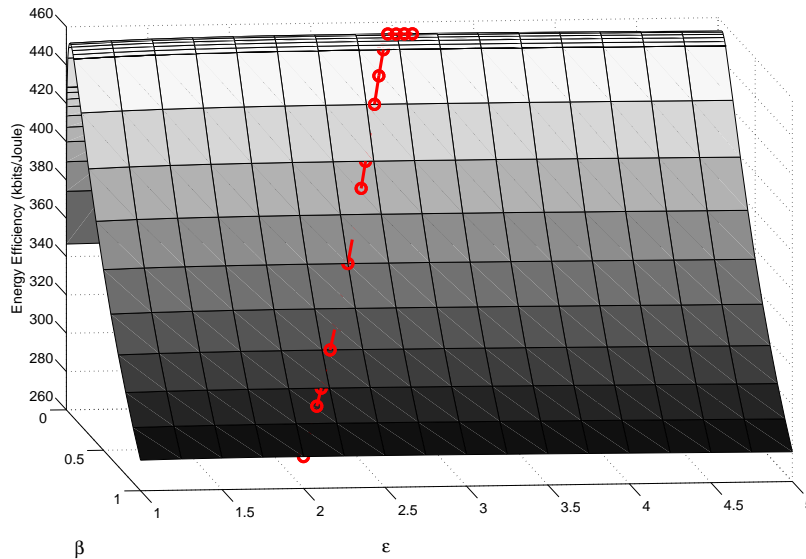


Figure 2. Illustration of the energy efficiency region of a sector and the proposed algorithm solutions per iteration using the gradient ascent method.

generating the pico eNBs and users, several minimum distance constraints are considered and these are presented in Table II, along with the other parameters and simulation models used in our numerical results. These parameters and channel models are in accordance with [14] for the baseline simulation of HetNets. Furthermore, we consider $\rho = 10^{-2}$ and $\mu_0 = 1/10$ in the gradient ascent power control algorithm.

Fig. 2 illustrates the energy efficiency of a sector for different (ε, β) pairs. The improvement of the proposed algorithm at each iteration is denoted by the red circles. Armijo rule is implemented to select the step sizes. As studied in Section III-A, this rule guarantees that energy efficiency increases at every iteration until it converges. Fig. 2 shows that the energy efficiency of the network is mostly affected by β . On the other hand, the effects of ε on energy efficiency is minor for the same β . This is expected since β determines the macrocell transmit power level which directly affects the total consumed power in the network, whereas ε does not change the total consumed power, but its effects are mostly observed on the total throughput.

In Figs. 3(a)-(b) and Figs. 4(a)-(b), we investigate the individual contributions of the methods to determine the cell-center boundaries, frequency scheduling, and power control gains for different schedulers. In Figs. 3(a)-(b) the EBW scheduler is studied and Figs. 4(a)-(b) depict the results

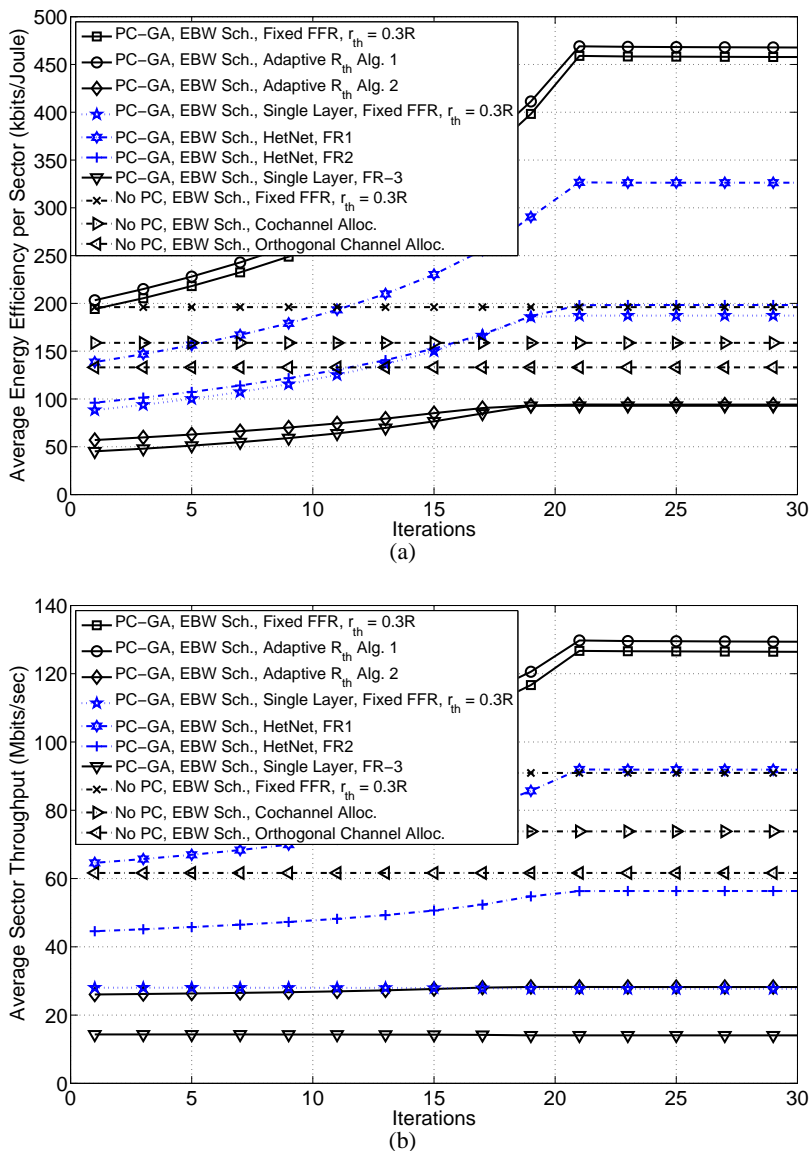


Figure 3. Average energy efficiency per sector (a) and average sector throughput (b) are depicted per iteration for the EBW scheduler.

for the SRM scheduler. The average energy efficiency of 57 sectors is plotted in Fig. 3(a) and Fig. 4(a), and the average sum throughput of sectors is depicted in Fig. 3(b) and Fig. 4(b). The proposed algorithm starts at full transmit power at the MeNB and iteratively updates ε and β along the derivative using the update rule in (19). The initial values are chosen as $(\varepsilon_0, \beta_0) = (2, 1)$. It can be observed that both the energy efficiency and throughput increase monotonically at each iteration.

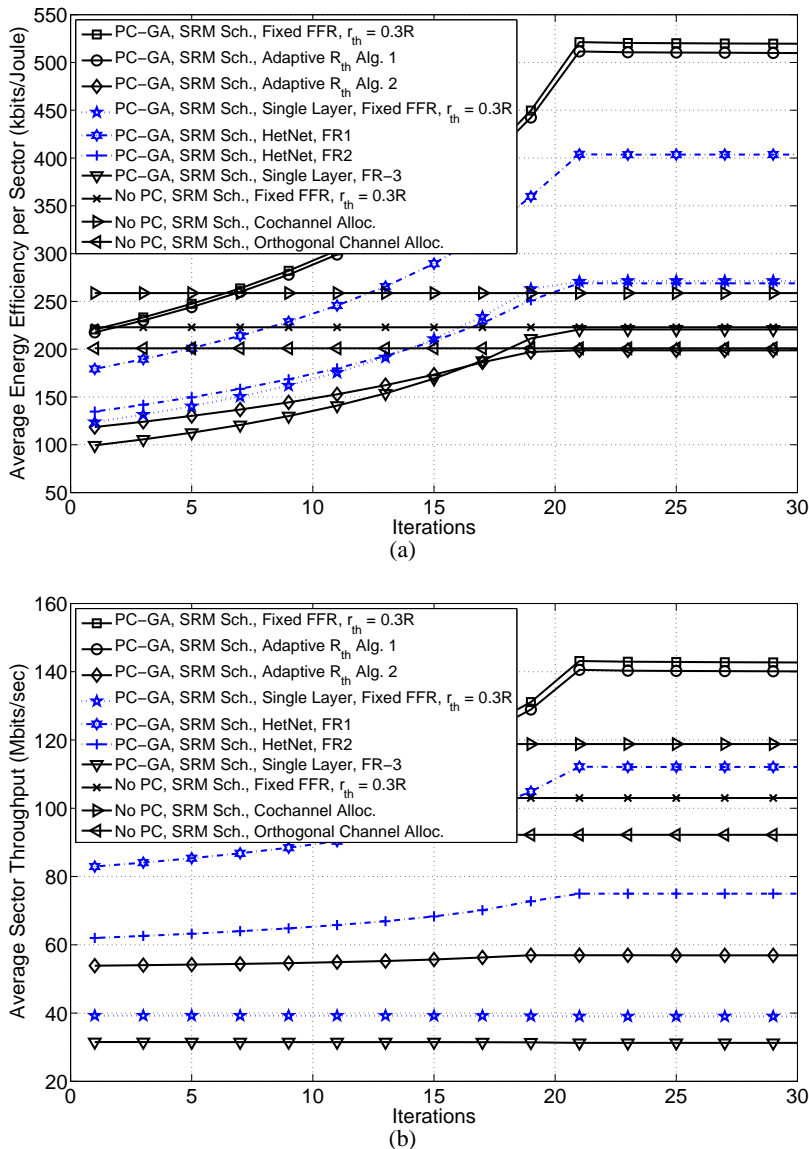


Figure 4. Average energy efficiency per sector (a) and average sector throughput (b) are depicted per iteration for the SRM scheduler.

Let us first identify the power control gain. In Fig. 3(a), when we compare the power control and no power control cases of the FFR spectrum allocation with EBW scheduler, it can be observed that the energy efficiency of the FFR spectrum allocation increases 2.38 times with the power control. In addition, we observe from Fig. 3(b) that power control brings a 37% throughput increase. Similar gains are observed with the SRM scheduler in Figs. 4(a)-(b) such that the energy efficiency gain is 2.29 times and the throughput gain is 40%. These gains are due

to adjusting the downlink transmit power and reducing both the intra- and inter-cell interference in the network. Notice that in Figs. 3(a)-(b) and Figs. 4(a)-(b) both the power control and no power control curves start almost at the same points and at each iteration we observe the power control curves monotonically increase their values indicating the power control gain.

Second, we analyze the effects of frequency scheduling on the energy efficiency. Comparing Fig. 3(a) and Fig. 4(a), we observe that the energy efficiency of the FFR scheme with the SRM scheduler is 10% better than that of the EBW scheduler. The throughput gain difference between these two schedulers is similar. This shows that the energy efficiency gain is mostly related to the throughput gain of the scheduler and the scheduler type has a relatively small effect on the power consumption.

Third, we analyze the performance of different spectrum allocation schemes in two-tiers. We observe that the FFR scheme outperforms the cochannel allocation by 24% and the orthogonal channel allocation by 47% in terms of energy efficiency. Similar gains are observed in the throughput performance as well. For the SRM scheduler, the cochannel allocation method has 20% better performance in both metrics compared to the orthogonal and FFR methods. This result, in fact, highlights the importance of the scheduler in use for different spectrum allocations.

Fourth, we compare the FR scheme to the FFR spectrum allocation in the HetNet architecture. We employ the proposed power control method and the SRM scheduler in both cases. As previously mentioned, two types of FR schemes in two-tier network are investigated. From Figs. 4(a)-(b), we observe that the energy efficiency of FR1 and FR2 are 269 and 403 kbits/Joule, respectively, whereas it is 510 kbits/Joule for the FFR allocation with adaptive cell-center regions. The average sector throughput of FR1, FR2, and FFR spectrum allocations are 75, 112.1 and 140.2 Mbits/sec, respectively. These results show that the FFR spectrum allocation provides 27–90% more energy efficient transmissions and 25–87% more throughput per sector compared to the FR spectrum allocation. These results also show that FFR is an effective spectrum allocation method that effectively utilizes the available spectrum by reducing the interference and increasing the achievable throughput. Similar conclusions can be drawn based on Figs. 3(a)-(b).

Fifth, we study the effects of the cell-center region boundaries. The proposed Adaptive R_{th}

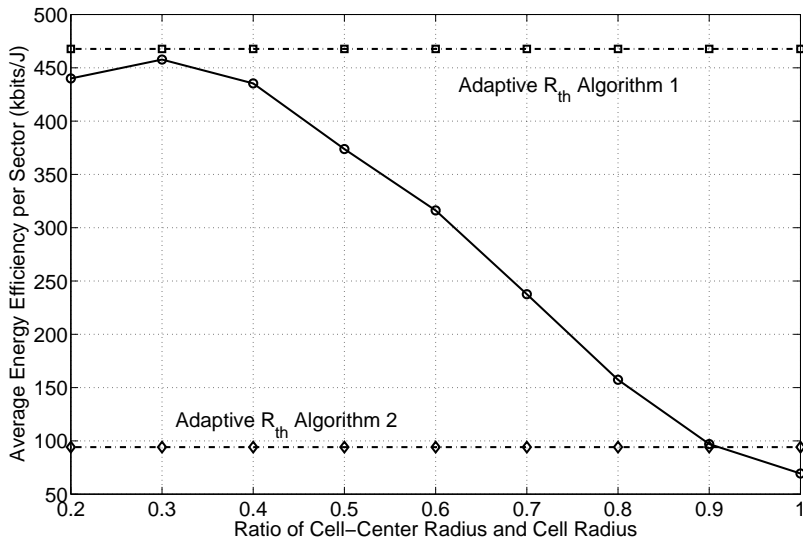


Figure 5. Average energy efficiency per sector versus the ratio of the cell-center region radius to cell radius.

Algorithm 1 has similar energy efficiency and throughput performance compared to the fixed radius FFR method with $r_{th} = 0.3R$ in both schedulers. However its performance is significantly higher compared to other constant radii values as depicted in Fig. 5 and Fig. 6.

Finally, we compare a single-tier macrocell only deployment to a HetNet architecture when the proposed power control method is applied along with the FFR scheme and the SRM scheduler. From Figs. 4(a)-(b), we observe that the energy efficiency of the single-layer network is 271 bits/Joule and it increases to 550 bits/Joule when picocells are deployed, indicating a 2x gain. Moreover, the spectral efficiency increases from 39 to 140 Mbits/sec from a single-layer to two-tier HetNet deployment, respectively. These results demonstrate the substantial gains that can be achieved with the picocell deployment. Again, similar conclusions can be drawn based on Figs. 3(a)-(b).

Fig. 5 shows the average energy efficiency per sector for different constant cell-center radii for the EBW scheduler. In this figure, the performance of the proposed adaptive R_{th} algorithms is also presented. First, we observe that the performance of the FFR system strictly depends on the cell-center region boundaries. For example, when the fixed radius FFR methods are considered and different radii values are enumerated, the system energy efficiency varies between 69 and 456

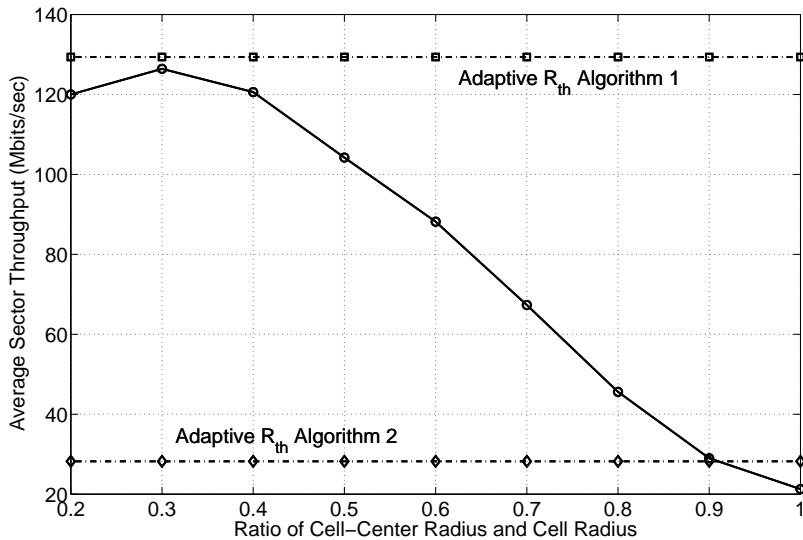


Figure 6. Average sector throughput versus the ratio of the cell-center region radius to cell radius.

kbits/Joule. Our simulation results show that the proposed Adaptive R_{th} Algorithm 1 outperforms all FFR methods with constant radii in both metrics. On the other hand, Adaptive R_{th} Algorithm 2 performs significantly worse as it prioritizes fairness rather than throughput. Note that there is a 5x gain between the two algorithms in terms of energy efficiency which illustrates the energy efficiency and fairness trade-off.

Fig. 6 compares the average sector throughput per sector of the fixed fractional cell-center radii to the adaptive R_{th} algorithms for the EBW scheduler. Similar to the energy efficiency, throughput performance strictly depends on the cell-center region boundaries such that the average sector throughput varies between 21 and 126 Mbps for different constant cell-center radii values. An important result is that the cell-center radius that maximizes the throughput is the same as that maximizes the energy efficiency. Note that these two radii are not necessarily the same. For example, with another power consumption model, these two radii can take different values.

V. CONCLUSION

Energy consumption of a wireless network is a serious concern for the next generation cellular networks such as LTE systems. To address this problem, we have proposed an energy-efficient resource allocation algorithm for OFDMA HetNet systems with the FFR scheme. The proposed

algorithm decouples the frequency and power allocation problems and successively solves each of them. It employs the gradient ascent method to solve the power allocation problem. The optimality conditions and the convergence of the proposed algorithm are also studied. Based on the simulation results, we show that the proposed algorithm significantly improves both the throughput and energy efficiency of the system. We also quantify the individual contributions of the effects of cell-center region, power control, and frequency scheduling gains in order to provide design guidelines. It is demonstrated that the proposed power control algorithm provides the most significant gains, while moderate gains can be achieved by different schedulers and adaptive cell-center region algorithms. Finally, we show that significant energy savings are also possible with the proposed algorithm which reduces the operational expenditures for the network operators and the Carbon footprint for the environment.

APPENDIX

In what follows, we prove that $\eta_i(\varepsilon, \beta)$ is quasiconcave in ε and β . It follows from Proposition 2 that $\eta_i(\varepsilon, \beta)$ is a quasiconcave function if and only if the following holds

$$\mathbf{y}^T \nabla \eta_i(\varepsilon, \beta) = 0 \text{ and } \mathbf{y}^T \nabla^2 \eta_i(\varepsilon, \beta) \mathbf{y} \leq 0 \quad (26)$$

where $\mathbf{y} = [y_1 \ y_2]^T$. First, we introduce new definitions for the proof, and then express the first and second order derivatives. Let $R_i(\varepsilon, \beta)$ denote the aggregate throughput of sector i which is given by

$$R_i(\varepsilon, \beta) = \sum_{k \in \mathcal{K}_M^C} \sum_{n \in \mathcal{N}_{M_k}^C} R_1^{(n)}(\varepsilon, \beta) + \sum_{k \in \mathcal{K}_M^X} \sum_{n \in \mathcal{N}_{M_k}^X} R_2^{(n)}(\varepsilon, \beta) + \sum_{k \in \mathcal{K}_P^X} \sum_{n \in \mathcal{N}_{P_k}^X \cap \mathcal{N}_M^C} R_3^{(n)}(\varepsilon, \beta) \quad (27)$$

where

$$\begin{aligned} R_1^{(k,n)}(\varepsilon, \beta) &= \log \left(1 + \frac{\beta a}{b + \varepsilon c} \right), & R_2^{(k,n)}(\varepsilon, \beta) &= \log \left(1 + \frac{\varepsilon \beta d}{b + \varepsilon c} \right) \\ R_3^{(k,n)}(\varepsilon, \beta) &= \log \left(1 + \frac{f}{\frac{\beta g}{b + \varepsilon c} + h} \right) \end{aligned} \quad (28)$$

where $a = P_{\max, M} g_{k, m}^{(n)} / I_k^{(n)}$, $b = N_M^C$, $c = N_M^X$, $d = P_{\max, M} g_{k, m}^{(n)} / (N_0 \Delta f)$, $f = P_{\max, P} / N_P^X g_{l, p}^{(n)}$, $g = P_{\max, M} g_{k, m}^{(n)}$, and $h = N_0 \Delta f$. Due to space considerations, we denote $R_i(\varepsilon, \beta)$, $R_1^{(k, n)}(\varepsilon, \beta)$, $R_2^{(k, n)}(\varepsilon, \beta)$, and $R_3^{(k, n)}(\varepsilon, \beta)$ by R_i , $R_1^{(k, n)}$, $R_2^{(k, n)}$, and $R_3^{(k, n)}$, respectively. Using these definitions, the first derivative of R_i with respect to ε can be expressed as

$$\frac{\partial R_i}{\partial \varepsilon} = \sum_{k \in \mathcal{K}_M^C} \sum_{n \in \mathcal{N}_{M_k}^C} \frac{\partial R_1^{(k, n)}}{\partial \varepsilon} + \sum_{k \in \mathcal{K}_M^X} \sum_{n \in \mathcal{N}_{M_k}^X} \frac{\partial R_2^{(k, n)}}{\partial \varepsilon} + \sum_{k \in \mathcal{K}_P^X} \sum_{n \in \mathcal{N}_{P_k}^X \cap \mathcal{N}_M^C} \frac{\partial R_3^{(k, n)}}{\partial \varepsilon} \quad (29)$$

where

$$\begin{aligned} \frac{\partial R_1^{(k, n)}}{\partial \varepsilon} &= -\frac{ac\beta}{(b+c\varepsilon)(a\beta+b+c\varepsilon)}, & \frac{\partial R_2^{(k, n)}}{\partial \varepsilon} &= \frac{bd\beta}{(b+c\varepsilon)(b+\varepsilon(c+d\beta))} \\ \frac{\partial R_3^{(k, n)}}{\partial \varepsilon} &= \frac{cfg\beta}{(h(b+c\varepsilon)+g\beta)((f+h)(b+c\varepsilon)+g\beta)}. \end{aligned} \quad (30)$$

The second derivative of R_i with respect to ε is given by

$$\frac{\partial^2 R_i}{\partial \varepsilon^2} = \sum_{k \in \mathcal{K}_M^C} \sum_{n \in \mathcal{N}_{M_k}^C} \frac{\partial^2 R_1^{(k, n)}}{\partial \varepsilon^2} + \sum_{k \in \mathcal{K}_M^X} \sum_{n \in \mathcal{N}_{M_k}^X} \frac{\partial^2 R_2^{(k, n)}}{\partial \varepsilon^2} + \sum_{k \in \mathcal{K}_P^X} \sum_{n \in \mathcal{N}_{P_k}^X \cap \mathcal{N}_M^C} \frac{\partial^2 R_3^{(k, n)}}{\partial \varepsilon^2} \quad (31)$$

where

$$\begin{aligned} \frac{\partial^2 R_1^{(k, n)}}{\partial \varepsilon^2} &= \frac{\beta ac^2 (a\beta + 2(b+c\varepsilon))}{(b+c\varepsilon)^2 (a\beta+b+c\varepsilon)^2} \\ \frac{\partial^2 R_2^{(k, n)}}{\partial \varepsilon^2} &= -\frac{bd\beta ((b+c\varepsilon)(2c+d\beta) + cd\varepsilon\beta)}{(b+c\varepsilon)^2 (b+\varepsilon(c+d\beta))^2} \\ \frac{\partial^2 R_3^{(k, n)}}{\partial \varepsilon^2} &= -\frac{c^2 fg\beta (2h(f+h)(b+c\varepsilon) + g\beta(f+2h))}{(h(b+c\varepsilon)+g\beta)^2 ((f+h)(b+c\varepsilon)+g\beta)^2}. \end{aligned} \quad (32)$$

Similarly, the first derivative of R_i with respect to β is

$$\frac{\partial R_i}{\partial \beta} = \sum_{k \in \mathcal{K}_M^C} \sum_{n \in \mathcal{N}_{M_k}^C} \frac{\partial R_1^{(k, n)}}{\partial \beta} + \sum_{k \in \mathcal{K}_M^X} \sum_{n \in \mathcal{N}_{M_k}^X} \frac{\partial R_2^{(k, n)}}{\partial \beta} + \sum_{k \in \mathcal{K}_P^X} \sum_{n \in \mathcal{N}_{P_k}^X \cap \mathcal{N}_M^C} \frac{\partial R_3^{(k, n)}}{\partial \beta} \quad (33)$$

where

$$\begin{aligned} \frac{\partial R_1^{(k, n)}}{\partial \beta} &= \frac{a}{a\beta+b+c\varepsilon}, & \frac{\partial R_2^{(k, n)}}{\partial \beta} &= \frac{d\varepsilon}{b+\varepsilon(c+d\beta)} \\ \frac{\partial R_3^{(k, n)}}{\partial \beta} &= -\frac{fg(b+c\varepsilon)}{(h(b+c\varepsilon)+g\beta)((f+h)(b+c\varepsilon)+g\beta)}. \end{aligned} \quad (34)$$

The second derivative of R_i with respect to β is given by

$$\frac{\partial^2 R_i}{\partial \beta^2} = \sum_{k \in \mathcal{K}_M^C} \sum_{n \in \mathcal{N}_{M_k}^C} \frac{\partial^2 R_1^{(k,n)}}{\partial \beta^2} + \sum_{k \in \mathcal{K}_M^X} \sum_{n \in \mathcal{N}_{M_k}^X} \frac{\partial^2 R_2^{(k,n)}}{\partial \beta^2} + \sum_{k \in \mathcal{K}_P^X} \sum_{n \in \mathcal{N}_{P_k}^X \cap \mathcal{N}_M^C} \frac{\partial^2 R_3^{(k,n)}}{\partial \beta^2} \quad (35)$$

where

$$\begin{aligned} \frac{\partial^2 R_1^{(k,n)}}{\partial \beta^2} &= -\frac{a^2}{(a\beta + b + c\varepsilon)^2}, & \frac{\partial^2 R_2^{(k,n)}}{\partial \beta^2} &= -\frac{d^2 \varepsilon^2}{(b + \varepsilon(c + d\beta))^2} \\ \frac{\partial^2 R_3^{(k,n)}}{\partial \beta^2} &= \frac{fg^2(b + c\varepsilon)((f + 2h)(b + c\varepsilon) + 2g\beta)}{(h(b + c\varepsilon) + g\beta)^2((f + h)(b + c\varepsilon) + g\beta)^2}. \end{aligned} \quad (36)$$

The derivative of R_i with respect to ε and β is

$$\frac{\partial^2 R_i}{\partial \varepsilon \partial \beta} = \sum_{k \in \mathcal{K}_M^C} \sum_{n \in \mathcal{N}_{M_k}^C} \frac{\partial^2 R_1^{(k,n)}}{\partial \varepsilon \partial \beta} + \sum_{k \in \mathcal{K}_M^X} \sum_{n \in \mathcal{N}_{M_k}^X} \frac{\partial^2 R_2^{(k,n)}}{\partial \varepsilon \partial \beta} + \sum_{k \in \mathcal{K}_P^X} \sum_{n \in \mathcal{N}_{P_k}^X \cap \mathcal{N}_M^C} \frac{\partial^2 R_3^{(k,n)}}{\partial \varepsilon \partial \beta} \quad (37)$$

where

$$\begin{aligned} \frac{\partial^2 R_1^{(k,n)}}{\partial \varepsilon \partial \beta} &= -\frac{ac}{(a\beta + b + c\varepsilon)^2}, & \frac{\partial^2 R_2^{(k,n)}}{\partial \varepsilon \partial \beta} &= \frac{bd}{(b + \varepsilon(c + d\beta))^2} \\ \frac{\partial^2 R_3^{(k,n)}}{\partial \varepsilon \partial \beta} &= \frac{cfg((f + h)h(b + c\varepsilon)^2 - g^2\beta^2)}{(h(b + c\varepsilon) + g\beta)^2((f + h)(b + c\varepsilon) + g\beta)^2}. \end{aligned} \quad (38)$$

The gradient of $\eta(\varepsilon, \beta)$ can be expressed as

$$\nabla \eta(\varepsilon, \beta) = \begin{pmatrix} \frac{\partial \eta(\varepsilon, \beta)}{\partial \varepsilon} \\ \frac{\partial \eta(\varepsilon, \beta)}{\partial \beta} \end{pmatrix} = \begin{pmatrix} \frac{\partial R_i}{\partial \varepsilon} \frac{1}{\psi} \\ \frac{\partial R_i}{\partial \beta} \frac{1}{\psi} - \frac{R_i}{\psi^2} \frac{\partial \psi}{\partial \beta} \end{pmatrix} \quad (39)$$

where

$$\frac{\partial R_i}{\partial \varepsilon} = \frac{\partial R_1}{\partial \varepsilon} + \frac{\partial R_2}{\partial \varepsilon} + \frac{\partial R_3}{\partial \varepsilon} \quad \text{and} \quad \frac{\partial R_i}{\partial \beta} = \frac{\partial R_1}{\partial \beta} + \frac{\partial R_2}{\partial \beta} + \frac{\partial R_3}{\partial \beta}. \quad (40)$$

Consider that $y^T \nabla \eta_i = 0$ is satisfied and use (39) to rearrange terms, we have

$$\frac{\partial R_i}{\partial \varepsilon} y_1 + \frac{\partial R_i}{\partial \beta} y_2 = \frac{\partial \psi}{\partial \beta} \frac{1}{\psi} R_i y_2. \quad (41)$$

The Hessian of η_i is given by

$$\nabla^2 \eta(\varepsilon, \beta) = \frac{1}{\psi} \begin{pmatrix} \frac{\partial^2 R_i}{\partial \varepsilon^2} & \frac{\partial^2 R_i}{\partial \varepsilon \partial \beta} - \frac{\partial R_i}{\partial \varepsilon} \frac{\partial \psi}{\partial \beta} \frac{1}{\psi} \\ \frac{\partial^2 R_i}{\partial \varepsilon \partial \beta} - \frac{\partial R_i}{\partial \varepsilon} \frac{\partial \psi}{\partial \beta} \frac{1}{\psi} & \Phi \end{pmatrix} \quad (42)$$

where

$$\Phi = \frac{\partial^2 R_i}{\partial \beta^2} - \frac{2}{\psi} \frac{\partial R_i}{\partial \beta} \frac{\partial \psi}{\partial \beta} - \frac{R_i}{\psi} \left(\frac{\partial^2 \psi}{\partial \beta^2} \right)^2 + 2 \frac{R_i}{\psi^2} \left(\frac{\partial \psi}{\partial \beta} \right)^2. \quad (43)$$

For the power consumption model in (13), $\frac{\partial^2 \psi}{\partial \beta^2} = 0$. When we expand the terms, we get

$$\mathbf{y}^T \nabla^2 \eta_i(\varepsilon, \beta) \mathbf{y} = \frac{\partial^2 R_i}{\partial \varepsilon^2} y_1^2 + 2 \left(\frac{\partial^2 R_i}{\partial \varepsilon \partial \beta} - \frac{\partial R_i}{\partial \varepsilon} \frac{\partial \psi}{\partial \beta} \frac{1}{\psi} \right) y_1 y_2 + \Phi y_2^2. \quad (44)$$

Substituting (41) in (44) and rearranging terms, we have

$$\mathbf{y}^T \nabla^2 \eta_i \mathbf{y} = \frac{1}{\psi} \left(\frac{\partial^2 R_i}{\partial \varepsilon^2} y_1^2 + 2 \frac{\partial^2 R_i}{\partial \varepsilon \partial \beta} y_1 y_2 + \frac{\partial^2 R_i}{\partial \beta^2} y_2^2 \right) = \frac{1}{\psi} \mathbf{y}^T \nabla^2 R_i \mathbf{y}. \quad (45)$$

where $\nabla^2 R_i$ denotes the Hessian of R_i . This means that η_i is quasiconcave if and only if R_i is quasiconcave. Next, we analyze the quasiconcavity of R_i . Using in (32), (36), and (38) in (45) to obtain $\mathbf{y}^T \nabla^2 R_i \mathbf{y} \leq 0$, we need to show that

$$\begin{aligned} & \sum_{k \in \mathcal{K}_M^C} \sum_{n \in \mathcal{N}_{M_k}^C} \left(\frac{\partial^2 R_1^{(n)}}{\partial \varepsilon^2} y_1^2 + 2 \frac{\partial^2 R_1^{(n)}}{\partial \varepsilon \partial \beta} y_1 y_2 + \frac{\partial^2 R_1^{(n)}}{\partial \beta^2} y_2^2 \right) \\ & + \sum_{k \in \mathcal{K}_M^X} \sum_{n \in \mathcal{N}_{M_k}^X} \left(\frac{\partial^2 R_2^{(n)}}{\partial \varepsilon^2} y_1^2 + 2 \frac{\partial^2 R_2^{(n)}}{\partial \varepsilon \partial \beta} y_1 y_2 + \frac{\partial^2 R_2^{(n)}}{\partial \beta^2} y_2^2 \right) \\ & + \sum_{k \in \mathcal{K}_P^X} \sum_{n \in \mathcal{N}_{P_k}^X \cap \mathcal{N}_M^C} \left(\frac{\partial^2 R_3^{(n)}}{\partial \varepsilon^2} y_1^2 + 2 \frac{\partial^2 R_3^{(n)}}{\partial \varepsilon \partial \beta} y_1 y_2 + \frac{\partial^2 R_3^{(n)}}{\partial \beta^2} y_2^2 \right) \leq 0. \end{aligned} \quad (46)$$

Notice that the summations in (46) are grouped into subcarriers based on their locations within the cell. The contributions of the cell-center and cell-edge MUEs are captured in the first two summations in (46), while the third is of the cell-edge PUEs. For the proof, it is necessary to show that the sum of these summations is non-positive.

First, we identify the condition for the first summation in (46), that is the terms for the

cell-center MUEs, as

$$\frac{\beta ac^2 (a\beta + 2(b + c\varepsilon))}{(b + c\varepsilon)^2} y_1^2 - 2acy_1y_2 - a^2y_2^2 \leq 0. \quad (47)$$

Adding and subtracting the term $(cky_1)^2$ from (47) and rearranging terms, we get

$$(\beta ac + c(b + c\varepsilon))^2 y_1^2 \leq (c(b + c\varepsilon)y_1 + a(b + c\varepsilon)y_2)^2. \quad (48)$$

Notice that this is the condition that relates to the cell-center MUEs.

Next, we investigate the condition for the second summation in (46) to hold, that is

$$-\frac{bd\beta((b + c\varepsilon)(2c + d\beta) + cd\varepsilon\beta)}{(b + c\varepsilon)^2} y_1^2 + 2bdy_1y_2 - d^2\varepsilon^2 y_2^2 \leq 0 \quad (49)$$

When we rearrange terms, we have the necessary condition for the cell-edge MUEs which is given by

$$2bd(b + c\varepsilon)^2 y_1y_2 \leq bd\beta((b + c\varepsilon)(2c + d\beta) + cd\varepsilon\beta) y_1^2 + d^2\varepsilon^2 (b + c\varepsilon)^2 y_2^2. \quad (50)$$

Finally, we see that the condition for the cell-edge PUEs is

$$\begin{aligned} & -c^2fg\beta(2h(f + h)(b + c\varepsilon) + g\beta(f + 2h))y_1^2 + 2cfdg((f + h)h(b + c\varepsilon)^2 - g^2\beta^2)y_1y_2 \\ & + fg^2(b + c\varepsilon)((f + 2h)(b + c\varepsilon) + 2g\beta)y_2^2 \leq 0. \end{aligned} \quad (51)$$

In our extensive simulations, we have observed that (47)-(51) are always satisfied. This makes us conjecture that R_i and η_i are negative semi-definite, as we have observed numerically. Therefore, we conclude that the function η_i should be quasiconcave in ε and β .

REFERENCES

- [1] K. Davaslioglu and E. Ayanoglu, "Quantifying potential energy efficiency gain in green cellular wireless networks," *IEEE Communications Surveys and Tutorials*, accepted for publication. Available on IEEE Xplore.
- [2] H. Holma and A. Toskala, *LTE-Advanced: 3GPP Solution for IMT-Advanced*. West Sussex, U.K.: John Wiley & Sons, Ltd, 2012.
- [3] C. Han *et al.*, "Green radio: Radio techniques to enable energy-efficient wireless networks," *IEEE Commun. Mag.*, vol. 49, no. 6, pp. 46–54, Jun. 2011.

- [4] E. Hossain, V. K. Bhargava, and G. P. Fettweis, *Green Radio Communication Networks*. Cambridge, U.K.: Cambridge Univ. Press, 2012.
- [5] J. Wu, S. Rangan, and H. Zhang, *Green Communications: Theoretical Fundamentals, Algorithms and Applications*. Boca Raton, FL, USA: CRC Press, 2013.
- [6] M. Assaad, "Optimal fractional frequency reuse (FFR) in multicellular OFDMA system," in *Proc. IEEE Veh. Technol. Conf. (VTC)*, Sep. 2008, pp. 1–5.
- [7] N. Saquib, E. Hossain, and D. I. Kim, "Fractional frequency reuse for interference management in LTE-Advanced HetNets," *IEEE Wireless Commun.*, vol. 20, no. 2, pp. 113–122, Apr. 2013.
- [8] G. Song and Y. Li, "Cross-layer optimization for OFDM wireless networks – Part I: Theoretical framework," *IEEE Trans. Wireless Commun.*, vol. 4, no. 2, pp. 614–624, Mar. 2005.
- [9] G. Miao, N. Himayat, and G. Li, "Energy-efficient link adaptation in frequency-selective channels," *IEEE Trans. Communications*, vol. 58, no. 2, pp. 545–554, Feb. 2010.
- [10] G. Miao, N. Himayat, G. Li, and S. Talwar, "Distributed interference-aware energy-efficient power optimization," *IEEE Trans. Wireless Commun.*, vol. 10, no. 4, pp. 1323–1333, Apr. 2011.
- [11] Z. Xu, G. Li, C. Yang, and X. Zhu, "Throughput and optimal threshold for FFR schemes in OFDMA cellular networks," *IEEE Trans. Wireless Commun.*, vol. 11, no. 8, pp. 2776–2785, Aug. 2012.
- [12] L. Hoo, B. Halder, J. Tellado, and J. Cioffi, "Multiuser transmit optimization for multicarrier broadcast channels: Asymptotic FDMA capacity region and algorithms," *IEEE Trans. Commun.*, vol. 52, no. 6, pp. 922–930, Jun. 2004.
- [13] K. Davaslioglu and E. Ayanoglu, "Efficiency and fairness trade-offs in SC-FDMA schedulers," *IEEE Trans. Wireless Commun.*, vol. 13, no. 6, pp. 2991–3002, June 2014.
- [14] 3GPP, TR 36.814, "Further advancements for E-UTRA physical layer aspects (Release 9)," Mar. 2010.
- [15] P. Marsch and G. P. Fettweis, *Coordinated Multi-Point in Mobile Communications: From Theory to Practice*. Cambridge, U.K.: Cambridge Univ. Press, 2011.
- [16] G. Auer *et al.*, "How much energy is needed to run a wireless network?" *IEEE Wireless Commun.*, vol. 18, no. 5, pp. 40–49, Oct. 2011.
- [17] F. Richter, A. Fehske, and G. Fettweis, "Energy efficiency aspects of base station deployment strategies for cellular networks," in *Proc. IEEE Veh. Technol. Conf.*, Sep. 2009, pp. 1–5.
- [18] H. Holtkamp, G. Auer, V. Giannini, and H. Haas, "A parameterized base station power model," *IEEE Commun. Letters*, vol. 17, no. 11, pp. 2033–2035, Nov. 2013.
- [19] Q. Li, R. Hu, Y. Xu, and Y. Qian, "Optimal fractional frequency reuse and power control in the heterogeneous wireless networks," *IEEE Trans. Wireless Commun.*, vol. 12, no. 6, pp. 2658–2668, Jun. 2013.
- [20] S. Boyd and L. Vanderberghe, *Convex Optimization*. Cambridge, U.K.: Cambridge Univ. Press, 2012.
- [21] D. P. Bertsekas, *Nonlinear Programming*. Belmont, MA: Athena Scientific, 1995.
- [22] E. Wolfstetter, *Topics in Microeconomics: Industrial Organization, Auctions, and Incentives*. New York: Cambridge Univ. Press, 2003.
- [23] K. Davaslioglu and E. Ayanoglu, "Interference-based cell selection in heterogeneous networks," in *Proc. Inform. Theory and Appl. (ITA) Workshop*, San Diego, CA, Feb. 2013, pp. 1–6.